Actin Paracrystals Display Double Schottky Diode-Like Electrical Behavior

Horacio F. Cantiello, Brenda C. Gutiérrez, and María del Rocío Cantero*

Actin filaments are abundant intracellular polymers implicated in cell motility and contraction. Actin also forms paracrystalline structures under various conditions, including exposure to lanthanides and other high ionic strength conditions. Here the electrical properties of purified actin paracrystals induced by either $MgCl_2$ or $GdCl_3$ are tested. Tight electrically seal-voltage-clamped crystals display strong rectification with a nonlinear conductance under symmetrical and biionic conditions, including 20 mM $GdCl_3$/140 mM KCl and 10 mM $MgCl_2$/140 mM KCl. Rectification is observed in symmetrical ionic conditions with positive-to-negative conductance ratios ranging from 4.18 to 9.00 nS. The current-to-voltage relationships can be fitted with theoretical double Schottky equations and resemble the behavior of semiconducting nanotubes. The highly nonlinear electrical properties of paracrystalline actin arrays may help explain the physiology of actin-rich cellular compartments, such as stereocilia of the cochlea and neuronal dendritic spines also suggest potentially relevant nano-technological properties of this protein.

1. Introduction

Actin filaments are essential cytoskeletal proteins that play a vital role in the contractile response of muscle cells and cellular movements in non-muscle cells. Actin is a highly conserved eukaryotic protein in most animals, plants, and fungi in multiple, tissue-specific, and developmentally regulated forms.[1] Filamentous actin (F-actin) is formed from globular or unpolymerized actin (G-actin).[2] Any elevation in ionic strength to physiological conditions (e.g., 2 mM $MgCl_2$/100 mM KCl) causes G-actin to readily polymerize into F-actin in a process thought to involve partial neutralization of surface charge by cation counterions present as neutral salts in the intracellular buffer.[3–6] Actin filaments are

H. F. Cantiello, B. C. Gutiérrez, M. del R. Cantero
Laboratorio de Canales Iónicos
Instituto Multidisciplinario de Salud
Tecnología y Desarrollo (IMSaTeD, CONICET-UNSE)
Santiago del Estero 4206, Argentina
E-mail: mcantero@conicet.gov.ar

linear polyelectrolytes whose charge density is much higher than expected by Manning's condensation theory.[7–11] This uncompensated charge has several significant biophysical and biological consequences, including a role in the electrostatic control of actin filament nucleation and elongation, bundling formation, and the binding and interaction with lipids, actin-binding proteins and microtubules.[6,7,12–18] The uncompensated charge may also explain the nonlinear electrical properties of F-actin, including its nonlinear electro-osmotic behavior and its ability to conduct ionic condensation-based waves.[10,19,20]

It has long been recognized that F-actin aggregates into paracrystalline structures as a result of the stepwise reduction of the net negative charge of actin monomers upon cation binding, where divalent cations are more effective than monovalent cations in the precipitation of actin.[21–24] Mg^{2+}-precipitated F-actin paracrystals consist of regularly packed filaments that retain the double-helical structures and correlate with the number of Mg^{2+} bound per mole of actin monomers.[4,25] $MgCl_2$ and polylysine/KCl form F-actin paracrystals and single-layered filament rafts.[26,27] The lanthanide Gadolinium (Gd^{3+}) also induces crystalline actin sheets and tubes where the inter-subunit contacts differ from those observed within F-actin.[28–32] The inter-subunit interactions of the F-actin monomers along the two long-pitch helical strands of filaments are conserved within the crystalline sheets. However, an unanticipated symmetry-breaking collective counterion mechanism has been found that generates attractions of multivalent ions on F-actin, such that counterions organize into "frozen" ripples parallel to the actin filaments, forming charge density waves.[33] This phenomenon agrees with surface potential microscopy measurements of actin bundles, where saturation of accumulated charges was observed, suggesting strong nonlinearity and periodicity in charge distribution about the polymer's surface.[34]

In the present study, we explored whether actin paracrystals induced by adding Gd^{3+} or Mg^{2+} (doping) into a high ionic strength KCl (140 mM) background solution have electrical properties consistent with semiconducting devices. Voltage-stimulated actin paracrystals were studied by the patch-clamp technique and behaved as semiconductors showing strong rectification that depended on the doped multivalent cation. Mg^{2+}-induced crystals displayed strongly symmetrical behavior that could be fitted with

a double heterojunction Schottky diode equation. The present data indicate that actin filaments form electrically active structures with strong semiconducting properties that may be implicated in novel intracellular signaling mechanisms.

2. Results

2.1. Actin Paracrystal Formation in the Presence of Different Cations

Actin crystals were grown spontaneously (**Figure 1**a) by overnight incubation in various solutions solely containing either $GdCl_3$ or $MgCl_2$ as initially reported (see **Table 1**) or the addition of the salts to an "intracellular" saline solution, as indicated in the Experimental Section and the Figures.[28–30] Overnight incubation in an intracellular solution without multivalent cations did not elicit crystal growth. Actin paracrystals were large and amorphous, reaching hundreds of μm in length (Figure 1a). The presence of actin in the crystals was confirmed by FITC-phalloidin labeling (Figure 1b).

The electrical activity of actin paracrystals was determined by the voltage clamp technique (Figure 1c), as reported for microtubule assemblies.[18,35,37] Control current-to-voltage relationships obtained with the pipette in solution in the absence of actin are shown for comparison in SupportingInformation. While the tip resistance of the patch pipette in symmetrical saline solution was, on average, 7.70 ± 0.44 MΩ ($n = 8$, range 5.7 to 10.0 MΩ), contact with the actin crystals produced an immediate higher-resistance seal in the order of 320 ± 152.7 MΩ ($n = 8$), with a range between 12.28 and 1207.7 MΩ.

Gadolinium-grown actin paracrystals patched in symmetrical KCl solution (patch pipette and bathing chamber) showed highly nonlinear currents in positive-to-negative potentials (**Figure 2**a). Strong rectification was observed under these conditions, with a rectification r factor of 9.00 (2.70 ± 0.20 nA V^{-1} vs. 0.30 ± 0.09 nA V^{-1}, $n = 12$) for positive versus negative biases, respectively. Paracrystals grown in the presence of $MgCl_2$ (Figure 2b) also showed rectification when patched in a symmetrical KCl so-

lution, with an $r = 4.18$ (4.60 ± 1.20 nA V^{-1}, $n = 31$ vs. 1.10 ± 0.60 nA V^{-1}, $n = 16$), for positive versus negative biases, respectively.

The Gd^{3+}-grown actin paracrystals also showed electrical rectification when patched in symmetrical $GdCl_3$ (20 mM) solution (**Figure 3**a), with a rectification r factor of 5.78 (133.1 ± 28.5 nA V^{-1}, $n = 8$ vs. 23.0 ± 8.7 nA V^{-1}, $n = 6$), for positive versus negative biases, respectively. Paracrystals grown in the presence of $MgCl_2$ (Figure 3b) and patched in the presence of KCl (140 mM) in the pipette and $MgCl_2$ (100 mM) in the bath solution showed strong rectification with $r = 7.72$ (44.0 ± 0.9 nA mV^{-1}, $n = 10$ vs. 5.70 ± 0.88 nA mV^{-1}, $n = 9$), for positive versus negative biases, respectively.

Interestingly, Mg^{2+}-grown crystals patched in symmetrical KCl 140 mM solution displayed strongly non-rectifying currents, which turned into double rectification in the presence of 10 mM $MgCl_2$ in the solution (**Figure 4**). Thus, divalent cations in the solution affected not only the formation of the paracrystal but also the electrical rectification pattern, suggesting that the voltage-induced addition of external divalent cations affected the electrical behavior of the crystal structure (Figure 4).

Actin paracrystals prepared and measured under symmetrical conditions in a solution containing 140 mM KCl and 10 mM $MgCl_2$ in both the pipette and the bath showed two typical responses without significant rectification (Figure 4a). First, a low conductance state was observed with an r of 0.89 (15.0 ± 1.9 nA V^{-1}, $n = 13$, vs. 17.1 ± 3.4 nA V^{-1}, $n = 13$) for positive versus negative biases, respectively. A high conductance state was also observed with an r of 0.93 (188.4 ± 21.0 nA V^{-1}, $n = 23$, vs. 202.0 ± 34.9 nA V^{-1}, $n = 18$) for positive versus negative biases, respectively (Figure 4b).

2.2. Double Schottky Diode Model of the Actin Paracrystal

To further understand the nature and magnitude of the rectification patterns of the actin paracrystals, an electrical model was developed that fitted with great accuracy the various experimental conditions (Figures 2–4). The electrical behavior observed in the current-to-voltage relationships of the actin paracrystals was consistent with a generalized heterojunction model

Table 1. Incubation, experimental conditions, slope conductance, and theoretical reversal potential (V_{rev}) for patch-clamped actin paracrystals. Values are the mean from 3–6 experiments.

Condition	Incubation conditions [mM]	Pipette/Bath Solution [mM]	Negative slope [nA V^{-1}]	Positive slope [nA V^{-1}]	Rectification Ratio [r]
1	500 $GdCl_3$	140 $KCl^{a)}$	0.30 ± 0.09	2.7 ± 0.22	9.00
4	100 $MgCl_2$	140 KCl/ 100 $MgCl_2$	5.70 ± 0.88	44.0 ± 0.9	7.72
6	20 $GdCl_3$	20 $GdCl_3$ $^{a)}$	23.0 ± 8.7	133.1 ± 28.5	5.78
8	140 KCl 10 $MgCl_2$	140 $KCl^{a)}$	1.10 ± 0.60	4.60 ± 1.20	4.18
11 – Low	140 KCl 10 $MgCl_2$	140 KCl 10 $MgCl_2$ $^{a)}$	17.1 ± 3.4	15.0 ± 1.9	0.88
11 – High	140 KCl 10 $MgCl_2$	140 KCl 10 $MgCl_2$ $^{a)}$	202.0 ± 34.9	188.4 ± 21.0	0.93

a) Indicates that both pipette and bath solutions contained the same ionic composition. Control current-to-voltage curves with the pipette are shown for comparison in Supporting Information.
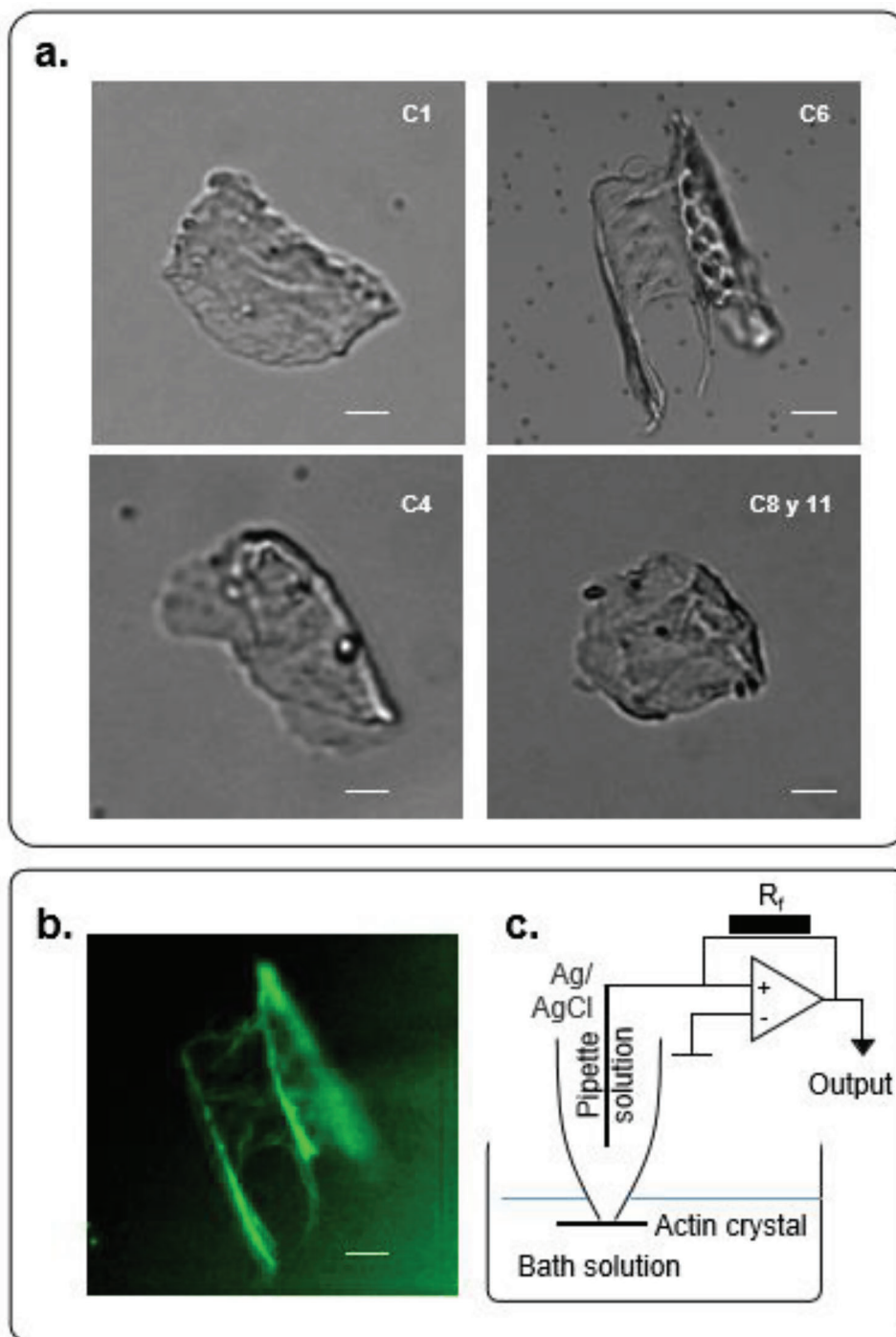
Figure 1. Paracrystals of purified actin. a) Examples of paracrystalline structures obtained by incubation of purified actin (1 mg mL^{-1}) under different conditions (Ci), from i = 1 to 8, as indicated in Table 1. DIC, X20, obtained images. b) Fluorescence image of FITC-phalloidin labeled actin paracrystal incubated under condition 6 (C6) with 20 mM GdCl$_3$ c). As indicated in the Experimental Section, schematics of the electric setup include the patch pipette that connects to the actin paracrystal in solution to a patch clamp amplifier. The horizontal bar represents 5 µm.

based on the following assumptions.[38–40] Usually, a regular metal/semiconductor device is described as a diode with two electrical junctions, an ohmic contact presenting a characteristic linear current–voltage (*I–V*) and a rectifying contact controlled by a potential barrier.[40–43] To better approach, our experimental results include two rectifying contacts, which could not be explained by the conventional analysis of *I–V* curves, such as the barrier model for electron motion in *n-n* heterojunctions devices.[45] More recently, a simple metal-insulator-semiconductor (MIS) back-to-back Schottky model was applied

**ADVANCED
SCIENCE NEWS**

www.advancedsciencenews.com

**ADVANCED
ELECTRONIC
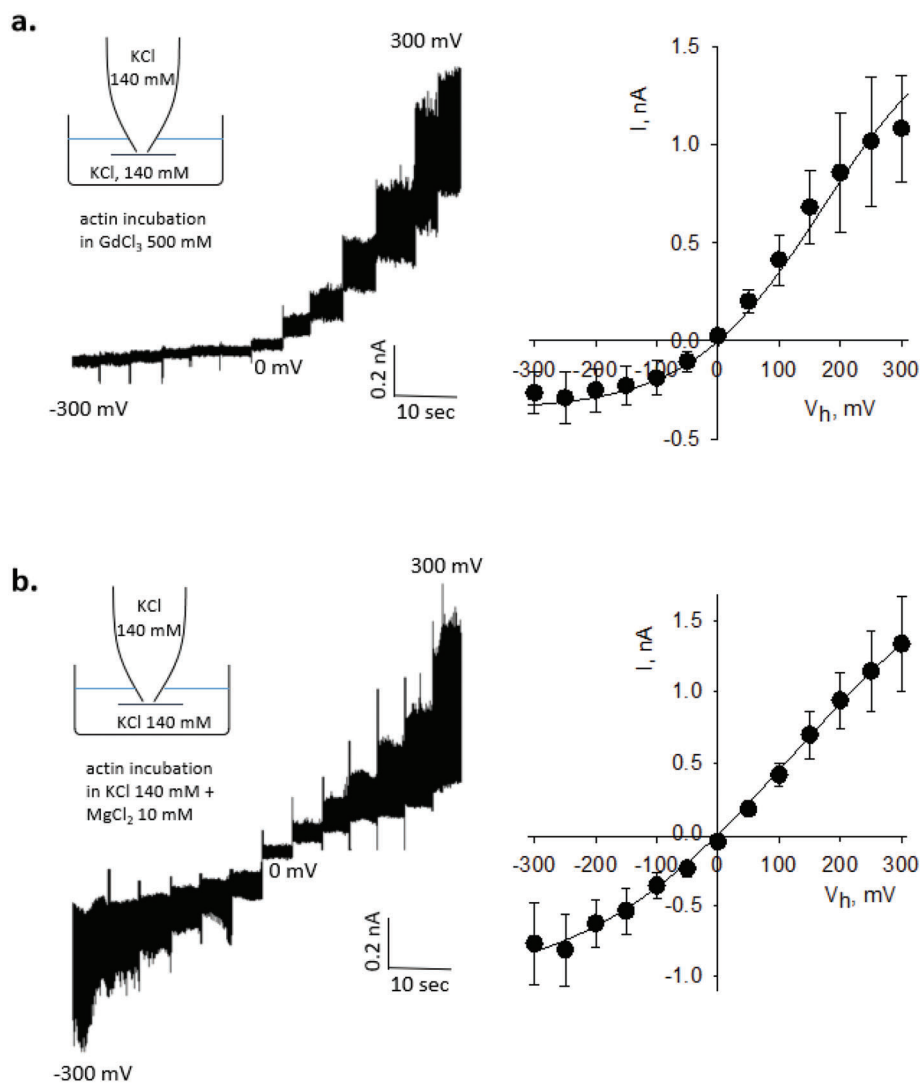MATERIALS**
Open Access

www.advelectronicmat.de

Figure 2. Electrical behavior of actin paracrystals. a) Left. The tracing shows the electrical currents produced by an actin paracrystal prepared in 500 mM $GdCl_3$ and measured in a symmetrical KCl (140 mM) solution. Applied holding potentials were between ±300 mV. Right. The plot indicates the current-to-voltage relationship of paracrystals under conditions on the Left. b) Left. The tracing shows electrical currents generated by an actin paracrystal prepared in KCl 140 mM and 10 mM $MgCl_2$ and measured in a symmetrical KCl (140 mM) solution. Applied holding potentials were between ± 300 mV. Right. The plot indicates the current-to-voltage relationship of experiments under conditions in Left. Data in both panels are the mean ± SEM (filled circles) from $n = 3$ and 11 experiments, respectively. The solid line is best fitting to Equation 3 under each condition. Details are indicated in the text, and values for the negative and positive slopes are shown in Table 1.

to nanowire devices, but the possibility of two different barriers was not considered.[46]

The effect of phalloidin was tested in the actin-containing KCl (140 mM) solution, which did not induce actin crystals, to ascertain whether the actin paracrystalline structure depended on the alignment of actin filaments in the assembled configuration. The presence of phalloidin readily formed large 2D-actin sheets (**Figure 5**). Patch clamping of these sheets disclosed important information about the process of voltage-induced rectification, which initiated as essentially linear (non-rectifying) currents that self-inhibited in only one direction (reverse bias), suggesting that negative potential-attraction of divalent cations to the crystal elicits the formation of a directional flow of cations through the structure.

A similar approach was used by Zhang et al. with a back-to-back model that included two different processes, both thermionic and field effect emission, for each barrier.[47] Although the assumption of varying transport processes for a single device may not be common, a two-Schottky barriers model has been applied to thin film transistors.[48]

2.3. Curve Fitting

Considering that in our experimental setup the actin paracrystal faces two interfaces in series, including the high ionic strength saline (both bath and patch pipette) with an AgCl metal interface for each electrode, the electrical behavior of the
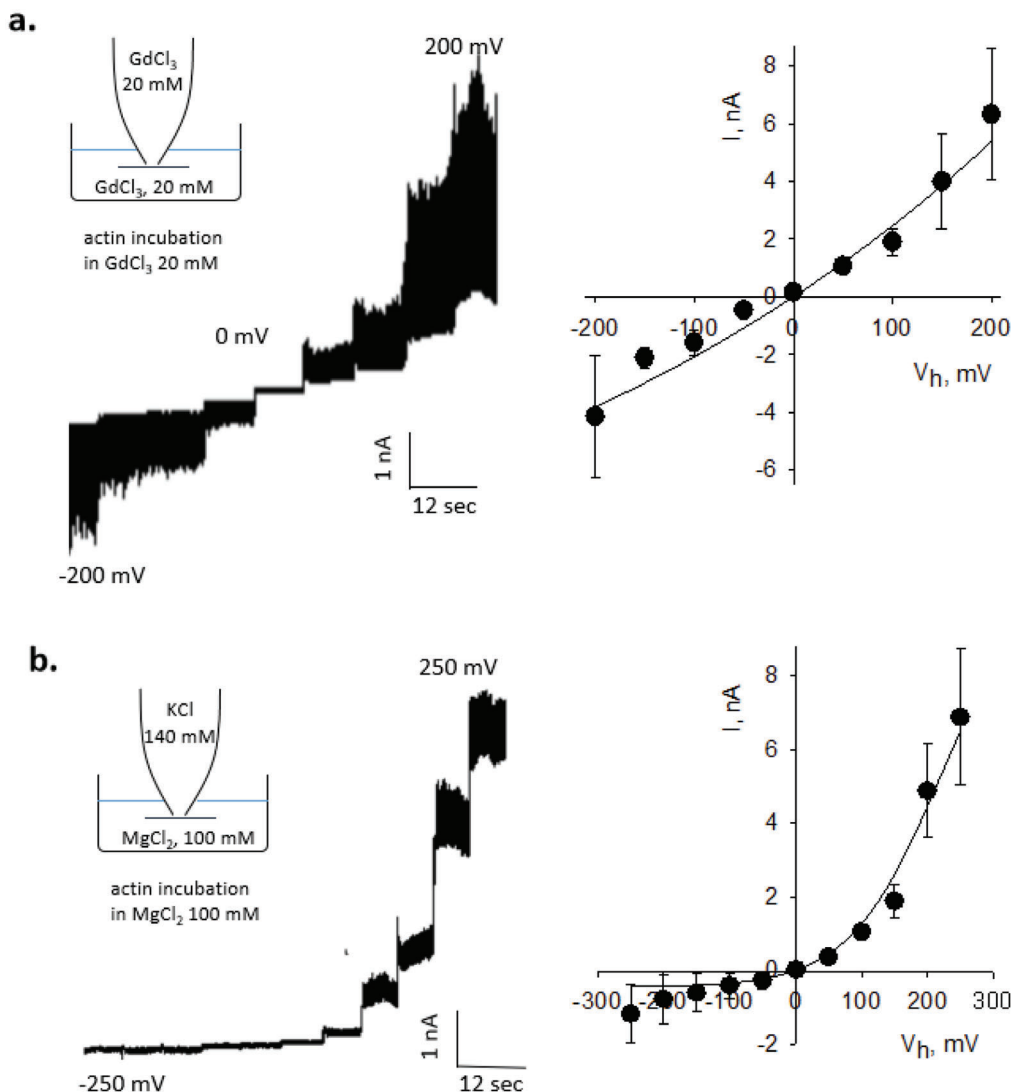
2300144 (4 of 9)

**ADVANCED
SCIENCE NEWS**

www.advancedsciencenews.com

**ADVANCED
ELECTRONIC
MATERIALS**

www.advelectronicmat.de

Figure 3. Electrical rectification of actin paracrystals is cation-dependent. a) Left. The tracing shows the temporal series of electrical currents generated by an actin paracrystal prepared in 20 mM GdCl$_3$ with the same solution in both pipette and bath (symmetrical conditions). Applied holding potentials were between ±200 mV. Right. The plot indicates the current-to-voltage relationship of experiments under conditions in Left. b) Left. The tracing shows the temporal series of electrical currents generated by an actin paracrystal prepared in 100 mM MgCl$_2$. Currents were measured in asymmetrical conditions, with a KCl (140 mM) solution in the pipette and the incubation solution in the bath (100 mM MgCl$_2$). The applied holding potential was between ±250 mV. Right. The plot indicates the current-to-voltage relationship of experiments under conditions in Left. Data in both Right panels are the mean ± SEM (filled circles) from $n = 8$ and 3 experiments, respectively. A solid line is the best fitting to Equation 3 under each condition. Details are indicated in the text, and values for the negative and positive slopes are shown in Table 1.

crystal was analyzed as having a metal/semiconductor/metal system. For this, a back-to-back double Schottky model consisting of two different barrier heights, the Ag^0/AgCl/saline/ Actin paracrystal /saline/AgCl/Ag^0 dual interface, was designed, following usual assumptions. Namely, each ideal diode current should decrease to a minimum value in a single barrier configuration. For the presence of two barriers, however, the applied voltage was thought of as being divided into two contributions across an equivalent circuit, closing a serial coupling of each element (barrier 1/actin crystal/barrier 2) such that the current in each barrier ($I_1 = -I_2$) also equaled the total current (I). Thus, the

current I in a metal/semiconductor heterojunction "i" could be written as:[44]

$$I_i = F \times \exp\left(-\frac{q^{\Phi_{B_i}}}{k_B T}\right) \exp\left(\frac{qV}{nk_B T}\right) \times \left[1 - \exp\left(-\frac{qV}{k_B T}\right)\right] \quad (1)$$

where F is a phenomenological constant that in normal diode behavior would include the Richardson constant times the square of the temperature, which in this case is also thought to be constant, Φ_{B_i} represents each Schottky barrier height ($i = 1, 2$), k_B
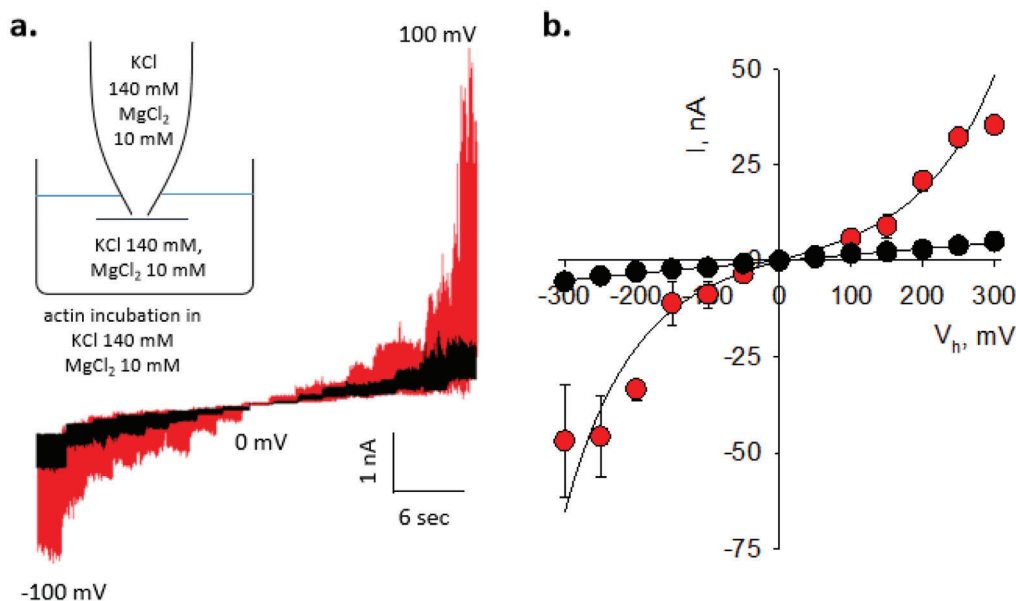
Figure 4. Effect of $MgCl_2$ on the electrical behavior of actin paracrystals. a) The tracings show the electrical currents generated by actin paracrystals prepared and measured in a solution containing 140 mM KCl and 10 mM $MgCl_2$ (symmetrical conditions). As indicated, two typical responses were observed: a lower (Black tracing) and higher (Red tracing) conductance with applied holding potentials between ±100 mV. b) The plot shows current-to-voltage relationships for both conductances on the Left (Black and Red circles, respectively). Data are the mean ± SEM (filled circles) from $n = 8$ and 9 experiments, respectively. The solid line is best fitting to Equation 3. Details are indicated in the text.

is the Boltzmann constant, q is the charge of the electron, and V, is the holding potential across the preparation. The effective barrier, following image-force effects, would always result in the voltage dependence of the barrier height, as follows:[49]

$$\Phi_{B_i} = \Phi_{B0i} + V_i \left(\frac{1}{n} - 1 \right). \qquad (2)$$

Where Φ_{B0i} is the value of each barrier in an ideal Schottky junction, and V_i is the voltage drop at the junction. The voltage dependence in Equation (2) would account for the interface states, and image-force lowering perturbs the electric field distribution at each metal/semiconductor interface affecting the barrier height. The model included the deviations of the Schottky barrier height as in either tunneling currents in highly doped materials or the generation-recombination in the space charge region, where the ideality factor has an essential contribution to the current-to-voltage relationship. Electrically speaking, because of the strong dependence of the bias signal of each Schottky barrier, the two diodes would be connected in their respective blocking (reverse bias) directions, where the total current (I) as a function
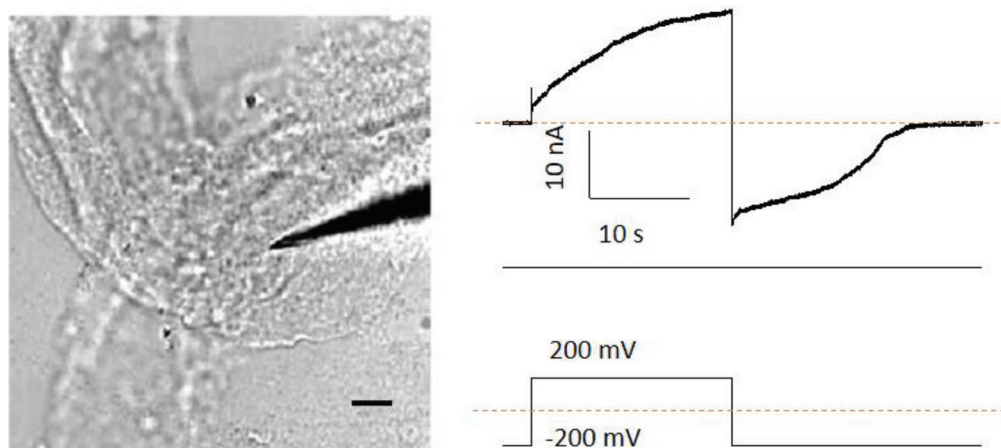

Figure 5. Electrical behavior of phalloidin-induced actin sheet. Left. Image of actin 2D-sheet induced by addition of FITC-phalloidin to an actin-containing solution in 500 mM $GdCl_3$ in the bath. DIC, X20, obtained images. The horizontal bar represents 20 μm. Right. Tracing shows the electrical current generated by the actin sheet in symmetrical KCl (140 mM). While initially linear, the current responds differently upon applying a positive potential (200 mV), which increases in time, decreasing and becoming strictly non-conducting at a negative potential (200 mV). Data are representative of three independent experiments. Dashed red lines indicate zero current (Top) or voltage (Bottom).

Table 2. Fitting parameters obtained with the double Schottky diode model.

Parameter→ ↓Condition	A	g	d	a	n	R*
1	2.8	1.1	2.4	10.0	3.0	0.9931
4	4.1	0.4	2.3	7.7	1.1	0.9950
6	4.1	0.9	1.4	11.8	1.1	0.9970
8	6.5	-1.8	1.1	0.8	1.0	0.9941
11 high	13.1	0.1	-0.3	5.03	0.8	0.9777
11 low	7.7	0.5	0.4	3.0	1.0	0.9976

of V, across the entire system, will be $I_1 = -I_2 = I$, similar to a condition where both metal–semiconductor–metal interfaces present a blocking effect, such that the current is written as

$$I(V) = \frac{I_{01} I_{02} \sinh\left(\frac{qV}{2k_BT}\right)}{I_{01}\exp\left(\frac{qV}{2k_BT}\right) + I_{02}\exp\left(\frac{-qV}{2k_BT}\right)} \quad (3)$$

Each $I_i = F \times \exp(-q\Phi_{Bi}/k_BT)$ (where $i = 1, 2$) can be regarded as similar to a generalization of the conventional current-to-voltage dependence in a metal/semiconductor device, representing two back-to-back Schottky diodes separated by the series resistance.

From the above, the electrical behavior of the actin paracrystal would behave as follows, when an external voltage (V) is applied to one terminal, one Schottky junction is forward biased while the second one is in reverse mode. Equation (3) provides the current-to-voltage characteristics of a diode with both a Schottky barrier and an ohmic contact ($\Phi_{B1} \neq \Phi_{B2} = 0$). As stated above, setting up $n = 1$ (ideal Schottky barriers) Equation (3) gives the current minimum (saturation values) for both direct and reverse polarization. Slight deviations from ideality, such as $n = 1.01–1.2$, commonly observed values, will help reproduce the effects of two barriers ($\Phi_{B1} = \Phi_{B2}$) on current flow through the structure.[44,49,50] As observed in diode heterojunctions, charge neutrality is determined by the nature of the semiconductor that regulates the charge transfer between the semiconductor and Fermi-level surfaces. The current-to-voltage relationships obtained for all experimental conditions in the present study were fitted with this model (Figures 2–4). The solid lines represent the best fitting obtained in each case. **Table 2** lists all parameters and coefficients obtained.

In conclusion, by replacing I_1 and I_2 in Equation 3, we obtain the following:

$$I(V) = \frac{\left[F\times\exp\left(-\frac{q\Phi_{B1}}{k_BT}\right)\right]\times\left[F\times\exp\left(-\frac{q\Phi_{B2}}{k_BT}\right)\right]\sinh\left(\frac{qV}{2k_BT}\right)}{\left[F\times\exp\left(-\frac{q\Phi_{B1}}{k_BT}\right)\right]\exp\left(\frac{qV}{2k_BT}\right) + \left[F\times\exp\left(-\frac{q\Phi_{B2}}{k_BT}\right)\right]\exp\left(\frac{-qV}{2k_BT}\right)} \quad (4)$$

and reordering

$$I(V) = F\frac{\exp\left(-\frac{q\Phi_{B1}}{k_BT}\right)\times\exp\left(-\frac{q\Phi_{B2}}{k_BT}\right)\sinh\left(\frac{qV}{2k_BT}\right)}{\exp\left(-\frac{q\Phi_{B1}}{k_BT}\right)\times\exp\left(\frac{qV}{2k_BT}\right) + \exp\left(-\frac{q\Phi_{B2}}{k_BT}\right)\times\exp\left(\frac{-qV}{2k_BT}\right)} \quad (5)$$

For simplification, we replaced $q\Phi_{B1}/k_bT$, $q\Phi_{B2}/k_bT$, and $q/2k_bT$ with -d, -g, and a, respectively. We also introduced the correction factor $(1+1/n)$ representing the drop of the voltage in the junction to obtain:

$$I(V) = F\frac{\exp(-d)\exp(-g)\sinh\left[aV\left(\frac{1}{n}+1\right)\right]}{\exp(-d)\exp(aV) + \exp(-g)\exp(-aV)} \quad (6)$$

3. Discussion

Here we demonstrated that paracrystals of purified actin act as semiconductors and most consistently respond to voltage with a double Schottky diode-like behavior. The data indicated that actin filaments aggregate with different cations (doping) to form electrically-active 3D units with highly nonlinear conductance in response to voltage bias. This is most evident in the phalloidin-induced 2D sheets (Figure 5), where the electrical response was initially linear to become strictly rectifying, consistent with the doping effect of the transferred ions into the paracrystalline structure. Several conditions bring about actin crystalline structures, including interactions with actin-binding proteins, where 3D co-crystals have been found both in vivo and in vitro.[51] The present study indicates that actin paracrystals bear a solid functional resemblance to the observed behavior of semiconducting nanowire- and nanobelt-based devices, and most interestingly, they follow the current-to-voltage relationship of double Schottky barrier devices very closely.[52–55] The response obtained in nanodevices produced under identical conditions and metallic contacts can differ significantly because the metal/semiconductor contacts depend largely on interfacial chemistry. The natural surface disorder of the structure can trap charges "spreading" the interface states into a few nanometers inside the semiconductor. Like regular metal/semiconductor devices, actin paracrystals behaved as diodes, with two electrical junctions: an ohmic contact and a rectifying contact. The transport properties of the protein complexes would implicate thermionic emission with the corrections required for two barriers for ion transport like the electron's motion in heterojunction devices, including a back-to-back Schottky model applied to nanowire devices.[45,46] A similar approach was used by Zhang et al., who considered both thermionic and field effect emissions for each barrier.[47] The assumption implies an enhanced tunneling probability as in highly doped metal–semiconductor barriers. The two Schottky barriers model has also been applied to thin film transistors to explain the effect of modified Au contacts on C60 films.[48] The electrical response of the 2D actin sheets bares a resemblance to this behavior and suggests that lateral coupling of actin filaments develops asymmetries upon ion doping, generating the rectifying phenomenon (Figure 5).

The molecular nature and biological relevance of this electrical behavior remain to be explored but may be relevant because various cytoskeletal actin structures display paracrystalline behavior. Paracrystalline arrays of actin have been identified in several biological compartments, including microvilli and the brush border, stereocilia, and the cuticular plate region of the cochlear hair cell, where they impart rigidity and stiffness which are essential for their sensory response properties. These structures

may also have an electrical contribution to cell function yet to be defined.[56–60]

Paracrystalline structures represent a relevant physical state of matter by being the "building blocks" of many materials, including biopolymers.[61] The possibility of semiconduction by proteins has been observed in many instances. However, the nature of the conductivity process in semiconductor proteins remains to be defined. Fuoss suggested an ionic conduction process, while Evans and later Rosemberg indicated that proteins would be electronic semiconductors.[62–64] Conversely, King and Medley found quantitative agreement with electrolysis theory, supporting the ionic-conduction process.[65] Cardew believed dry proteins would be electronic semiconductors while wet proteins would be proton current carriers.[66] Thus far, no information on the semiconductor properties of proteins such as actin in solution is available. The details of how charge carrier transport occurs will depend on the details of the dielectric constant on the activation energy in the ionic semiconductor. For the case of proteins, the immediate neighborhood of any change in the structure remains to be defined. The expectation is, however, that an electronic charge removed from a protein monomer would require work to accomplish the change between ionization energy and electron affinity. The inserted electric charge in a previously neutral dielectric region will polarize the medium and induce an electrostatic potential on the charge. The work necessary to separate the two charges (the electron and the hole, each of which polarizes the medium) is the semiconduction activation energy for the dry protein. The effective dielectric constant of the medium will increase by water absorption of the protein, such that the new activation energy in the wet state is reduced.

The present study provides evidence for the cation-induced nonlinear electric behavior of actin paracrystals, which may have significant physiological consequences for cell signaling by the actin cytoskeleton. Highly organized actin structures also offer the possibility of developing protein-based novel electronic devices.

4. Experimental Section

Actin Polymerization: Actin was polymerized as previously reported.[10] Briefly, actin from rabbit muscle origin (Catalog # A2522 Sigma Aldrich, St. Louis, MO) was dissolved at 1 mg mL^{-1} in distilled water per the manufacturer's recommendation. Actin paracrystals were obtained by overnight incubating an aliquot of the actin solution in either 100 mM $MgCl_2$ or 500 mM $GdCl_3$. When indicated, FITC-phalloidin (Catalog # P5282, Sigma Aldrich, St. Louis, MO) was added to the patch-clamp chamber to stabilize actin and detect the structures under study by fluorescence.

Microscopy: Actin structures were viewed with an Olympus IX71 inverted microscope connected to a digital CCD camera C4742-80-12AG (Hamamatsu Photonics K.K., Bridgewater, NJ). Whenever indicated, actin preparations were also stained with FITC-phalloidin (Sigma Aldrich, St. Louis, MO) and observed under fluorescence microscopy. Images were collected on a Dell-NEC personal computer using the IPLab Spectrum acquisition and analysis software (Scanalytics, Viena, VA). Final composite images were created using ImageJ software (National Institutes of Health, USA).

Electrophysiology: Electrophysiology of actin paracrystals was conducted as recently reported for sheets of brain microtubules.[35] Unless otherwise stated, actin paracrystals were voltage clamped under symmetrical conditions, with an "intracellular" Ca^{2+} free solution containing

(in mM): KCl 140, NaCl 5, EGTA 1.0, and HEPES 10, adjusted to pH 7.2 with KOH, in both the patch pipette and the bathing chamber. An aliquot of the actin-containing solution was seeded onto a clean glass surface at the bottom of a patch clamping chamber under DIC microscopy. Electrical signals were obtained, filtered, and digitized with a miniaturized patch-clamp amplifier (ePatch, Elements Inc, Cesena, Italy), with ±500 mV and ±200 nA, voltage and current range, respectively, and a maximum signal bandwidth response of 100 kHz. Patch pipettes were made from soda-lime capillaries (Biocap, Buenos Aires, Argentina) with a 1.25 mm internal diameter. Pipette tips were pulled with a pipette puller (PB-7, Narishige Tokyo, Japan) and fire polished (MF-9, Narishige Tokyo, Japan) to a 3–4 μm tip diameter. Electrical signals were stored in a personal computer with the software Elements Data Reader 3.0 (Elements, Cesena, Italy) and later analyzed with Clampfit 10 (Molecular Devices, San José, CA, USA). Sigmaplot Version 11.0 (Systat Software Inc, CA, USA) was used for statistical analysis and graphics.

Statistics: Unless otherwise stated, values were expressed as the mean ± SEM (n = the number of experiments), and comparisons were carried out as intergroup Student's t-test, with a significance of $p < 0.05$.[36]

Conflict of Interest

The authors declare no conflict of interest.

Data Availability Statement

The data that support the findings of this study are available from the corresponding author upon reasonable request.

[1] E. S. Hennessey, D. R. Drummond, J. C. Sparrow, *Biochem. J.* **1993**, *291*, 657.

[2] J. A. Cooper, E. L. Buhle, S. B. Walker, T. Y. Tsong, T. D. Pollard, *Biochemistry* **1983**, *22*, 2193.

[3] M. Kawamura, K. Maruyama, *J. Biochem. (Tokyo)* **1970**, *68*, 885.

[4] A. Martonosi, C. M. Molino, J. Gergely, *J. Mol. Chem.* **1964**, *239*, 1057.

[5] W. F. H. M. Momntserts, *J. Biol. Chem.* **1952**, *198*, 459.

[6] F. Oosawa, S. Asakura, K. Hotta, N. Imai, T. Ooi, *J. Polym. Sci. Part D. Macromol. Rev.* **1959**, *37*, 323.

[7] J. X. Tang, P. A. Janmey, *J. Biol. Chem.* **1996**, *271*, 8556.

[8] S. Kobayasi, *Biochim. Biophys. Acta* **1964**, *88*, 541.

[9] S. Kobayasi, H. Asai, F. Oosawa, *Biochim. Biophys. Acta* **1964**, *88*, 528.

[10] H. F. Cantiello, C. Patenaude, K. Zaner, *Biophys. J.* **1991**, *59*, 1284.

[11] G. S. Manning, *Q. Rev. Biophys.* **1978**, *11*, 179.

[12] F. Oosawa, *Biopolymers* **1970**, *9*, 677.

[13] A. H. Crevenna, N. Naredi-Rainer, A. Schönichen, J. Dzubiella, D. L. Barber, D. C. Lamb, R. Wedlich-Söldner, *J. Biol. Chem.* **2013**, *288*, 12102.

[14] L. Rioux, C. Gicquaud, *J. Ultrastruc. Res.* **1985**, *93*, 42.

[15] D. St-Onge, C. Gicquaud, *Biochem. Cell Biol.* **1989**, *67*, 297.

[16] A. Renault, P. F. Lenne, C. Zakri, A. Aradian, C. Vénien-Bryan, F. Amblard, *Biophys. J.* **1999**, *76*, 1580.

[17] K. J. Amann, B. A. Renley, J. M. Ervasti, *J. Biol. Chem.* **1998**, *273*, 28419.

[18] M. R. Cantero, B. C. Gutierrez, H. F. Cantiello, *Cytoskeleton* **2020**, *77*, 167.

[19] E. C. Lin, H. F. Cantiello, *Biophys. J.* **1993**, *65*, 1371.

[20] J. A. Tuszynski, S. Portet, J. M. Dixon, C. Luxford, H. F. Cantiello, *Biophys. J.* **2004**, *86*, 1890.

[21] A. Vazina, G. Frank, B. Lemazhtkhin, *J. Mol. Biol.* **1965**, *14*, 373.

[22] K. Yamamoto, M. Yanagida, M. Kawamura, K. Maruyama, H. Noda, *J. Mol. Biol.* **1975**, *91*, 463.

[23] H. Strzelecka-Gołaszewska, W. Drabikowski, *Biochim. Biophys. Acta – Bioenergetics* **1968**, *162*, 581.

[24] H. Strzelecka-Golaszewska, E. Prochniewicz, W. Drabikowski, *Eur. J. Biochem.* **1978**, *88*, 219.

[25] J. Hanson, *Proc. R. Soc. Lond B* **1973**, *183*, 39.

[26] P. R. Smith, W. E. Fowler, T. D. Pollard, U. Aebi, *J. Mol. Biol.* **1983**, *161*, 641.

[27] W. E. Fowler, U. Aebi, *J. Cell. Biol.* **1982**, *93*, 452.

[28] C. G. dos Remedios, M. J. Dickens, *Nature* **1978**, *276*, 731.

[29] U. Aebi, P. R. Smith, G. Isenberg, T. D. Pollard, *Nature (Lond)* **1980**, *288*, 296.

[30] U. Aebi, W. E. Fowler, G. Isenberg, T. D. Pollard, P. R. Smith, *J. Cell Biol.* **1981**, *91*, 340.

[31] M. O. Steinmetz, K. N. Goldie, U. Aebi, *J. Cell Biol.* **1997**, *138*, 559.

[32] M. O. Steinmetz, A. Hoenger, P. Tittmann, K. H. Fuchs, H. Gross, U. Aebi, *J. Mol. Biol.* **1998**, *278*, 703.

[33] T. E. Angelini, H. Liang, W. Wriggers, G. C. L. Wong, *Proc. Natl. Acad. Sci. USA* **2003**, *100*, 8634.

[34] P. Zhang, H. F. Cantiello, *App. Phys. Lttrs.* **2009**, *95*, 033701.

[35] M. R. Cantero, P. L. Perez, M. Smoler, C. Villa Etchegoyen, H. F. Cantiello, *Sci. Rep.* **2016**, *6*, 27143.

[36] G. W. Snedecor, W. G. Cochran, *Statistical Methods*, Iowa State University Press, Ames, Iowa **1973**.

[37] M. R. Cantero, C. Villa Etchegoyen, P. L. Perez, N. Scarinci, H. F. Cantiello, *Sci. Rep.* **2018**, *8*, 11899.

[38] X. L. Tang, H. W. Zhang, H. Su, Z. Y. Zhong, *Physica E* **2006**, *31*, 103.

[39] C. J. Dalmaschio, O. M. Berengue, D. G. Stroppa, R. A. Simon, A. J. Ramirez, W. Herwig Schreiner, A. J. Chiquito, E. R. Leite, *J. Cryst. Growth.* **2010**, *312*, 1860.

[40] A. J. Chiquito, C. A. Amorim, O. M. Berengue, L. S. Araujo, E. P. Bernardo, E. R. Leite, *J. Phys.: Condens. Matter* **2012**, *24*, 225303.

[41] J. Bardeen, *J. Phys. Rev.* **1947**, *71*, 717.

[42] R. T. Tung, *Mater Sci Eng R* **2001**, *35*, 1.

[43] J. F. Wager, *Thin Solid Films* **2008**, *516*, 1755.

[44] S. M. Sze, *Physics of Semiconductor Devices*, Wiley, New York **1981**.

[45] W. G. Oldham, A. G. Milnes, *Solid-State Electron.* **1964**, *7*, 153.

[46] F. Hernández-Ramírez, A. Tarancon, O. Casals, J. Rodríguez, A. Romano-Rodríguez, J. R. Morante, S. Barth, S. Mathur, T. Y. Choi, D. Poulikakos, *Nanotechnol* **2006**, *17*, 5577.

[47] Z. Zhang, K. Yao, Y. Liu, C. Jin, X. Liang, Q. Chen, L. M. Peng, *Adv. Funct. Mater.* **2007**, *17*, 2478.

[48] T. Nagano, M. Tsutsui, R. Nouchi, N. Kawasaki, Y. Ohta, Y. Kubozono, C. Takahashi, A. Fujiwara, *J. Phys. Chem.* **2011**, *C111*, 7211.

[49] E. H. Rhoderick, *Metal Semiconductor Contacts*, Clarendon Press, Oxford **1988**.

[50] T. Nishimura, K. Kita, A. Toriumi, *Appl. Phys. Lttrs.* **2007**, *91*, 123123.

[51] H. G. Mannherz, *J. Biol. Chem.* **1992**, *267*, 11661.

[52] J. Kong, N. R. Franklin, C. W. Zhou, M. G. Chapline, S. Peng, K. J. Cho, H. J. Dai, *Science* **2000**, *287*, 622.

[53] C. Li, D. H. Zhang, X. L. Liu, S. Han, T. Tang, J. Han, C. W. Zhou, *Appl. Phys. Lett.* **2002**, *82*, 1613.

[54] H. Q. Liu, J. Kameoka, D. A. Czaplewski, H. G. Craighead, *Nano Lettrs* **2004**, *4*, 671.

[55] A. Grillo, A. Di Bartolomeo, *Adv. Electron. Dev.* **2021**, *7*, 2000797.

[56] J. A. Spudich, L. A. Amos, *J. Mot. Biol.* **1979**, *129*, 319.

[57] J. W. Brown, C. J. McKnight, *PLoS One* **2010**, *5*, e9406.

[58] L. G. Tilney, D. J. Derosier, M. J. Mulroy, *J. Cell Biol.* **1980**, *86*, 244.

[59] J. C. Saunders, M. E. Schneider, S. P. Dear, *J. Acoust. Soc. Am.* **1985**, *78*, 299.

[60] D. Drenckhahn, K. Engel, D. Höfer, C. Merte, L. Tilney, M. Tilney, *J. Cell Biol.* **1991**, *112*, 641.

[61] A. M. Hindeleh, R. Hosemann, *J. Phys. C: Solid State Phys.* **1988**, *21*, 4155.

[62] R. M. Fuoss, *J. Am. Chem. Soc.* **1939**, *61*, 2329.

[63] M. G. Evans, J. Gergely, *Biochim. Biophys. Acta* **1949**, *3*, 188.

[64] B. Rosenberg, *J. Chem. Phys.* **1962**, *36*, 816.

[65] G. King, J. A. Medley, *J. Colloid. Sci.* **1949**, *4*, 1.

[66] M. H. Cardew, D. D. Eley, *Discuss. Faraday. Soc.* **1957**, *27*, 115.